Sustainable Energy & Fuels

ROYAL SOCIETY OF CHEMISTRY

PAPER

View Article Online
View Journal | View Issue

Cite this: *Sustainable Energy Fuels*, 2025, **9**, 5619

Back to black: utilizing unsupported Pt for thin cathodes in PFSA-free PEM fuel cells

Hannes Liepold, [ab] Hendrik Sannemüller, [c] Philipp A. Heizmann, [a] Julian Stiegeler, [a] Tym de Wild, [bc] Carolin Klose, [ac] Robert Alink, [d] Severin Vierrath, [ab] Steven Holdcroft [e] and Andreas Münchinger *[ac]

Received 10th June 2025
Accepted 28th August 2025

DOI: 10.1039/d5se00809c

rsc.li/sustainable-energy

In hydrocarbon-based proton exchange membrane fuel cells, cathode catalyst layers (CLs) made from fluorine-free, sulfonated polyphenylenes (*e.g.*, Pemion®) face challenges in balancing sufficient gas transport with low protonic resistance – a tradeoff that is especially pronounced at application-relevant low humidity operation. Here, we address this issue by utilizing unsupported Pt, *i.e.*, platinum black (PtB), as the electrocatalyst to reach very thin CLs (<2.5 μm). When compared to CLs with carbon-supported platinum (Pt/C), evaluation at the same roughness factor (rf) reveals a performance increase from 180 to 420 mA cm^{-2} at 0.75 V, 50% RH and 95 °C, which is the highest reported performance for a fuel cell with hydrocarbon membrane and CLs and on par with perfluorosulfonic acid reference cells. Accelerated Pt dissolution tests reveal a fast initial rf loss within the first 100 potential cycles for PtB compared to Pt/C (15% *vs.* 4%), but virtual identical after 30 000 cycles.

Introduction

Hydrocarbon (HC)-based proton exchange membrane (PEM) fuel cells present a fluorine-free[1,2] alternative to conventional fuel cells based on perfluorosulfonic acids (PFSAs). While PFSAs are known for their unique combination of excellent ionic conductivity and high chemical stability in the acidic fuel cell environment,[3] their sustainability remains a challenge. As part of the per- and polyfluoroalkyl substances (PFAS) group, growing concerns over their toxicity and impact on both human and animal health have driven the European Chemicals Agency (ECHA) to assess potential regulatory restrictions on PFSAs.[4,5] The use of proton-conductive HC materials as membranes and electrode binders is considered a promising alternative to PFSAs, potentially providing environmental benefits that support the advancements of next-generation fuel cell development.[6] However, the HC ionomer-containing cathode catalyst layer (CL) faces challenges in balancing oxygen transport resistance with protonic conductivity. This tradeoff is especially pronounced at low relative humidity (RH),[7,8] and remains, along with the high kinetically induced overpotentials (*e.g.* platinum poisoning),[9–13] a main obstacle to market launch. Although HC polymers exhibit inherently low gas permeability[14–16] and are susceptible to excessive swelling,[6,17] their potential in PEM fuel cells has been demonstrated under favorable conditions (*i.e.*, H_2/O_2, 100% RH, $T < 90$ °C).[9,12,18–22] However, performance issues due to incomplete CL utilization arise at drier, application-relevant operating conditions[8] (*i.e.*, H_2/Air, ≤ 50% RH, $T > 90$ °C), where the ionomer's bulk[1,23] and thin film[8] proton conductivity is reduced compared to PFSAs. To avoid a complex ionomer redesign, recent studies using sulfonated phenylated polyphenylenes have attempted to reduce the cathode's protonic resistance without altering the chemistry of the ionomer. The approaches range from ionomer gradients in the cathode CL[7] to the production of CLs with reduced thickness (*e.g.*, by altering the Pt-on-carbon ratio[8]). Reducing the cathode CL thickness, as also shown for PFSA-based CLs,[24,25] reduces both protonic resistance and gas transport resistance, thereby offering the potential to close the remaining performance gap between HC- and PFSA-based electrodes.

In this report, we investigate the performance of ultra-thin (<2.5 μm) cathode CLs in fully HC-based fuel cells under application-relevant, low-humidity conditions. Our approach employs a sulfonated polyphenylene ionomer in combination with unsupported platinum nanoparticles, platinum black (PtB), as an electrocatalyst. Historically, PtB-based CLs with high platinum loading (~4 mg Pt cm^{-2}) and non-proton-conductive binders (*e.g.*, PTFE) were commonly used in early fuel cell designs in the late 1980s.[26,27] However, limited Pt utilization shifted the focus to PFSA-impregnated CLs with carbon-supported electrocatalysts.[28,29] In parallel, thin CLs have been investigated, *e.g.*, using 3M's nanostructured thin film (NSTF) catalysts,[24] but they faced challenges related to water management and

[a]*Electrochemical Energy Systems, IMTEK Department of Microsystems Engineering, University of Freiburg, Georges-Köhler-Allee 103, 79110 Freiburg, Germany*

[b]*Freiburg Materials Research Center (FMF), University of Freiburg, Stefan-Meier-Straße 21, 79104 Freiburg, Germany*

[c]*Hahn-Schickard-Gesellschaft für angewandte Forschung e.V., Georges-Köhler-Allee 103, 79110 Freiburg, Germany*

[d]*Aerostack GmbH, Max-Eyth-Strasse 2, 72581 Dettingen an der Ems, Germany*

[e]*Department of Chemistry, Simon Fraser University, Burnaby, BC V5A 1S6, Canada*

fabrication.[30,31] Here, we revisit the use of PtB in combination with hydrocarbon ionomers. We provide evidence that ultra-thin CLs based on this approach can overcome the longstanding tradeoff between mass transport and protonic resistance under application-relevant conditions.

Methods

Materials

Two sulfonated phenylated polyphenylene ionomers with different transport properties were utilized in electrodes based on hydrocarbons (HC): (i) biphenyl-linked sulfonated phenylated polyphenylene (sPPB, Fig. 1a)[1,2] provided by the Holdcroft group and (ii) Pemion® PP1-HNN8-00-X (known as HNN8, Ionomr Innovations Inc, Fig. 1b). The ion exchange capacity (IEC) of sPPB was titrated as 3.3 ± 0.1 meq g^{-1} (reported in literature[1] as 3.19 meq g^{-1}), while Pemion® HNN8 had an IEC of 3.1 ± 0.1 meq g^{-1}. Nafion (D2020, DuPont, polymer dispersion) was the ionomer used in PFSA-based electrodes.

Catalyst inks were prepared by mixing purified water, isopropanol (IPA), electrocatalyst, and ionomer solution, followed by ultrasonication (Hielscher UIS250L, 100 W, one hour, cooled in an ice bath). HC solutions consisted of 5 wt% ionomers, dispersed in a 1 : 1 mass ratio of IPA : H_2O (stirred for 24 hours at 40 °C and 260 rpm). To uncover the tradeoff between protonic resistance and gas transport resistance in the cathode CL (initial study), an electrocatalyst (TEC10E50E, Tanaka Kikinzoku Kogyo) with 46.6 wt% platinum supported on Ketjenblack (Pt/C) was mixed with different wt% of sPPB and Nafion. In the subsequent performance analysis, HC-based cathodes featured HNN8 with different electrocatalysts: (i) TEC10E50E and (ii) unsupported Pt (PtB, The Fuel Cell Store). Depending on the electrocatalyst, different ionomer-to-carbon ratios (I/C) were adjusted, namely I/C = 0.2 (TEC10E50E) and 2.5 wt% ionomer in solids (PtB). The PFSA reference cathode utilizes TEC10E50E with an I/C ratio of 0.8. In all studies, anodes featured TEC10E50E with an I/C ratio of 0.2 (HC) and 0.8 (PFSA).

Membrane electrode assembly (MEA) preparation

HC inks were spray-coated (Sono-Cell®, Sonaer Inc.) onto a Pemion® membrane (PF1-HLF8-15-X, Ionomr Innovations Inc., mechanically-reinforced) with a thickness of 15 μm, while PFSA inks were deposited onto a short side-chain Fumapem FS-715-RFS membrane (15 μm, Fumatech GmbH, mechanically-reinforced). Anodes featured a constant Pt loading of 0.1 mg_{Pt} cm^{-2}, while the Pt loading on the cathode was adjusted to 0.4 mg_{Pt} cm^{-2} (Pt/C), 1.2 mg_{Pt} cm^{-2} (PtB, degradation tests) or 1.6 mg_{Pt} cm^{-2} (PtB, protonic and gas transport resistance analysis and performance measurements). The final Pt loading was confirmed *via* X-ray fluorescence spectroscopy measurements (μXRF, M4 Tornado, Bruker Corporation). Two polyethylene naphthalate foils (CMC61325, CMC Klebetechnik GmbH), each with a thickness of 40 μm, were used as sub-gaskets and laminated onto catalyst-coated membranes (CCMs) to create an active geometric area of 4 cm^2 and reduce mechanical failure. A gas diffusion medium (Freudenberg H14Cx653) with a thickness of 185 μm and a serpentine flow field (Scribner Associates Inc.) was used on the anode and cathode. A final compression ratio of 20% was ensured using PTFE-coated fiberglass gaskets (Fiberflon®, assumed to be incompressible), each with a thickness of 110 μm, and an assembly torque of 10 Nm.

In situ characterization

All membrane electrode assemblies (MEAs) were tested using a commercial test stand (850e Fuel Cell Test System, Scribner Associates) equipped with an external potentiostat with frequency analyzer (Interface 5000E™, Gamry Instruments). Before starting the electrochemical characterization, all MEAs were conditioned using a voltage-controlled break-in procedure (80 °C, 96% RH, and ambient pressure under 0.25/1 slpm H_2/O_2), cycling the cell potential from open circuit voltage (OCV) to 0.3 V, to 0.6 V, and back to OCV. Each voltage step was held for one minute and repeated 20 times in total.[9] No recovery protocol was used in this study.

The roughness factor rf (cm_{Pt}^2 cm_{MEA}^{-2}) was determined from voltammograms obtained by cyclic voltammetry measurements (CVs) with fully 0.2 slpm humidified H_2 gas flow on the anode and no gas flow on the cathode. The measurements were conducted at ambient pressure and 40 °C. Thereby, the potential was scanned eight times back and forth from 0.05 V to 1.0 V with a scan rate of 50 mV s^{-1}. The rf was calculated by normalizing the integrated hydrogen adsorption

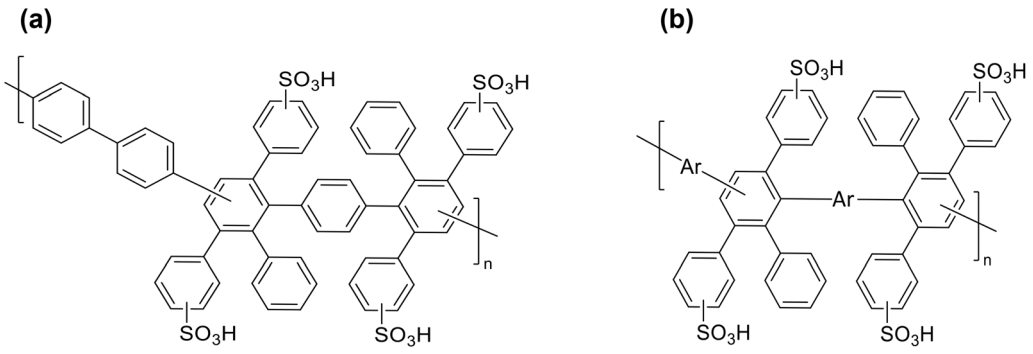

Fig. 1 Structure of (a) biphenyl-linked sulfonated phenylated polyphenylene (sPPB) and (b) Pemion®, both variations of sulfonated phenylated polyphenylenes.

charge (averaged over the last four cycles) with a specific charge of 210 μC cm_{Pt}^{-2}. The ECSA was calculated by dividing the obtained rf by the Pt loading. Before the initial measurement, two cleaning cycles were applied.

Impedance spectroscopy measurements in H_2/N_2 (0.5/0.5 slpm) at 50% RH, 80 °C, 1.5 bar_{abs}, and an amplitude of 22.5 mV were performed to estimate the cathode's protonic resistance R_{H^+} (*via* a fit of the impedance response to a 1D transmission line model). The applied voltage was set to 0.45 V, while the frequency was scanned from 100 kHz to 0.2 Hz (20 points per decade). Subsequently, the protonic resistivity r_{H^+} of the cathode was obtained by normalizing R_{H^+} with the CL thickness obtained from *ex situ* cross-section measurements (see below for details regarding the CL thickness measurements).

The total oxygen transport resistance was measured following the procedure outlined in Baker *et al.*[32] Limiting current measurements were performed at 80 °C, 80% RH under differential flow conditions with 1 slpm H_2 (anode). The gas flow on the cathode was set to 4 slpm using a gas mixture containing 0.5% O_2 in the rest of N_2. The cell potential was set to 0.4 V, 0.3 V, 0.2 V, 0.15 V, and 0.1 V for 120 s each. Measurements with different pressures were conducted (*i.e.*, 1.65, 2.15, 2.65, 3.2 bar_{abs}, where the pressure equals the average pressure from cell inlet to cell outlet), to extract the pressure-independent gas transport resistance $R_{O_2}^{indep}$ from the total gas transport resistance R_{O_2}.

The mass activity i_m and specific activity were assessed under H_2/O_2 (0.25/1.0 slpm) at 80 °C, 96% RH, and 1.5 bar_{abs} by measuring polarization curves from 0 mA cm^{-2} to 95 mA cm^{-2} (*i.e.*, current-controlled measurement). With a hold time of three minutes per data point, measurement ranges of 0–30 mA cm^{-2} with steps of 2.5 mA cm^{-2} and 35–95 mA cm^{-2} with steps of 15 mA cm^{-2} were applied. The measured voltage was corrected for the high-frequency resistance (R_{HFR}, measured at 3200 Hz), while the current density was adjusted by the shorting current of the membrane and the hydrogen-crossover current.[33] Both the shorting and crossover currents were determined from linear sweep voltammetry (LSV) measurements at 80 °C, 96% RH, and 1.5 bar_{abs} under H_2/N_2 (0.20/0.05 slpm). After applying the corrections, (i) the mass activity equals the Pt loading-normalized current density at a potential of 0.9 $V_{HFR\text{-}corrected}$ and (ii) the specific activity equals the mass activity normalized to the ECSA.

H_2/Air (0.25/1 slpm) polarization curves were recorded at 95 °C, 2.5 bar_{abs}, and 50% RH from low to high current density (*i.e.*, current controlled). The current range was 0–0.25 A (steps of 0.0125 A), 0.375 to 2 A (steps of 0.125), and 2.25 to 25 A (steps of 0.25 A, with a determination at 0.4 V). Each current density was held for three minutes, while the voltage used for evaluations corresponded to the average value taken within the last ten seconds.

A voltage-cycling-based accelerated stress test (AST) was conducted at 80 °C, 95% RH, ambient pressure, and H_2/N_2 (0.05/0.02 slpm) gas flows. To accelerate the loss in rf, a trapezoidal-wave-cycle potential was applied. The voltage was cycled between 0.6 V and 0.95 V, with each potential held for 2.5 s and a ramp time of 0.5 s. Intermediate measurements were performed at 100, 1000, 10k, and 30k cycles.

Ex situ characterization

Cross sections of the used cathode CLs were prepared using a focused ion beam (FIB) scanning electron microscope (FE-SEM, Amber X, Tescan GmbH). The samples were first cut in liquid nitrogen and then mounted onto standard aluminum SEM stubs (Science Services GmbH) using conductive double-sided adhesive carbon tabs. Protective carbon layers were deposited on the areas of interest using FIB deposition. Ablation was performed with FIB, milling a width of approximately 100 μm using Xe^+ ions at 20 kV acceleration voltage and a current of 10 nA, followed by polishing with 100 pA. Micrographs of the cathode CLs were taken at an acceleration voltage of 2 kV, a working distance of around 6 mm, and a current of 100 pA using an Everhart–Thornley (ET) detector. For quantitative thickness analysis, the micrographs were adjusted for the acquisition angle (52°) and segmented with the Trainable Weka Segmentation plugin for ImageJ. After binarization with Weka, the layer thicknesses were measured in increments of a minimum of 0.05 μm to produce thickness histograms.

Results

HC-based fuel cell performance: the bottleneck at low RH

For Nafion-based CLs with Pt/C it has been shown that the optimum performance is obtained for both wet and dry conditions using an ionomer to carbon ratio (I/C) of 0.8 that balances well protonic and gas transport resistance.[22,34] This corresponds to a dry volume fraction $\varepsilon_{i,\,dry}^{PFSA}$ of 0.14. However, optimal performance for HC-based CLs is achieved with significantly lower ionomer content, as confirmed by polarization curve measurements (Fig. 2a). When studying mass transport related limitations, it needs to be noted that not only the operation conditions such as the gas flow rate have impact on the high current performance of HC-based cathodes (see SI, Fig. S5b), but the preconditioning of such electrodes may fundamentally restructure the ionomer distribution and thereby change their electrochemical properties.[35] Furthermore, HC ionomers are still under development and batch-to-batch variations regarding purity and molecular weight (affecting catalyst poisoning or ionomer swelling) are expected to occur. Apart from these disclaimers and limitations on universality, the pressure-independent gas transport resistance $R_{O_2}^{indep}$ can be associated with the local transport resistance through the ionomer and the Knudsen diffusion in the pore network. Under conditions with low oxygen molar fraction on the cathode (*i.e.*, 0.5% O_2 in the rest of N_2), $R_{O_2}^{indep}$ of the best performing Nafion-based CL (I/C = 0.8) is determined to be 0.22 s cm^{-1} (Fig. 2b). To not exceed this value for HC-based cathode CLs, the volume fraction of dry HC ionomer is limited to $\varepsilon_{i,\,dry}^{HC} \leq 0.06$, corresponding to an I/C ratio of 0.2, which is currently often used in literature.[7,9,11,17] However, with high cathode gas flow rates and extensive conditioning procedures, also higher I/C ratios are reported.[36,37] As the HC ionomer experiences more pronounced swelling than the PFSA ionomer when exposed to hot water,[6,38] the CL is expected to be more sensitive towards liquid water generated during the oxygen reduction reaction.

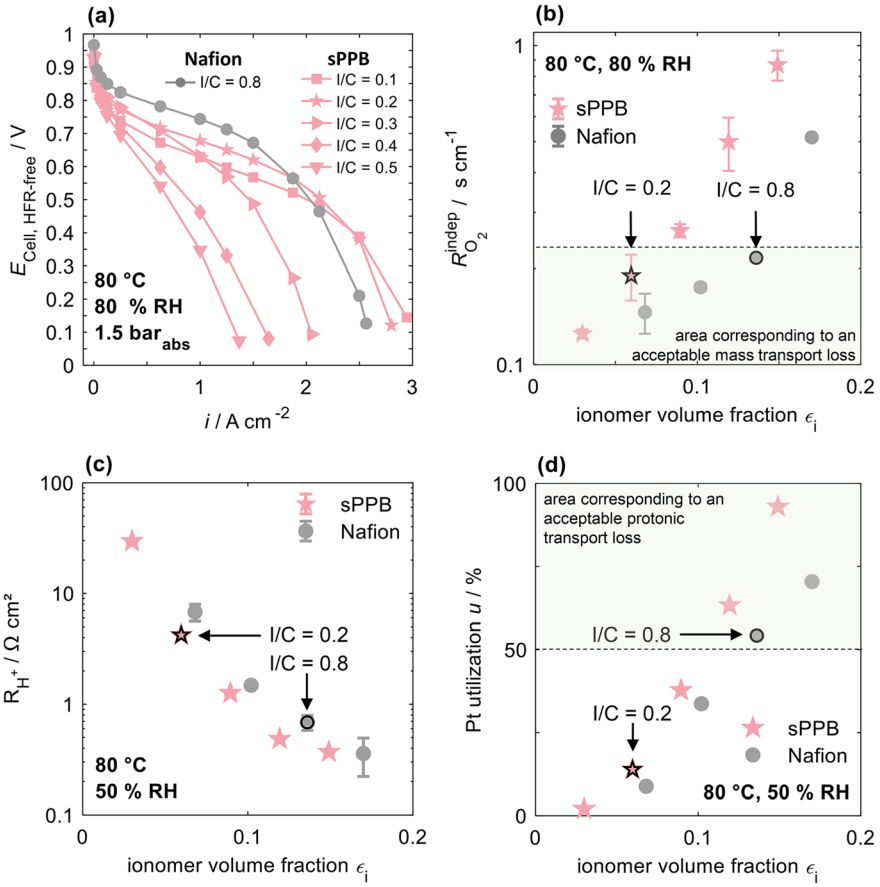

Fig. 2 Comparison of Nafion- and sPPB-based cathode CLs with varying I/C ratios/dry ionomer volume fractions ε_i: (a) HFR-free polarization curves at 80 °C, 1.5 bar_{abs} and 80% RH under H_2/Air (0.25/1 slpm); (b) pressure-independent O_2 transport resistance $R_{O_2}^{indep}$ at 80 °C and 80% RH; (c) protonic resistance R_{H^+} at 80 °C and 50% RH, extracted under H_2/N_2 (0.5/0.5 slpm); (d) protonic resistance-induced Pt utilization u at 80 °C and 50% RH. Black framed data points refer to the "standard" I/C ratio of operation.

This increased swelling contributes to the higher mass transport-induced overpotential observed in the system.[36] At mass transport optimized HC ionomer contents (*i.e.*, I/C = 0.2 or $\varepsilon_{i,\ dry}^{HC} = 0.06$), the protonic resistance R_{H^+} of sPPB-based cathodes is 4.2 Ω cm^2 at 50% RH, which is almost one order of magnitude higher compared to cathode CLs based on Nafion (*i.e.*, 0.69 Ω cm^2 at I/C = 0.8 or $\varepsilon_{i,\ dry}^{PFSA} = 0.14$) – see therefore Fig. 2c. The high proton transport resistance R_{H^+} results in a highly non-homogeneous current distribution perpendicular through the CL. Subsequently, the protonic resistance-induced catalyst utilization near the gas diffusion medium is determined to be 14%, which is significantly below the assumed threshold of 50% required for acceptable electrode performance. The catalyst utilization was calculated following the study of Neyerlin *et al.*[39] and Liepold *et al.*[8] at 50 mA cm^{-2}, assuming a single intrinsic Tafel slope of 70 mV dec^{-1} and a transfer coefficient of 1. Consequently, HC-based CLs with 50 wt% Pt/C and a Pt loading higher than 0.4 mg_{Pt} cm^{-2} do not improve in performance at low RH (≤50%), despite the increased number of reaction sites.[8] This poses a challenge for future applications of fully HC-based fuel cells. A refined balance between protonic resistance and mass transport resistance is required to compete with the performance of PFSA-based CLs under dry conditions.

HC-based fuel cell performance: the impact of CL thickness

Among low kinetic induced overpotentials, low protonic resistance, combined with sufficient gas transport resistance in HC-based cathode CLs, is key to high electrode performance. Both resistances are known to alter with the thickness of the electrode.[40,41] Recently, the influence of CL thickness on protonic resistance and catalyst utilization was systematically investigated in electrodes using a Pt/C electrocatalyst with HC ionomer.[8] The study showed a significant performance improvement under application-relevant low humidity conditions when the Pt/C ratio was increased from 50 wt% to 70 wt%, while maintaining a constant Pt loading. However, the extent to which the Pt/C content can be increased is limited, placing a lower boundary on the achievable CL thickness and its associated resistances. To address this limitation, CLs utilizing PtB are expected to allow for even thinner electrodes with potentially higher ionomer contents, achieving a more favorable ionomer tortuosity. Hence, thin CLs should enable

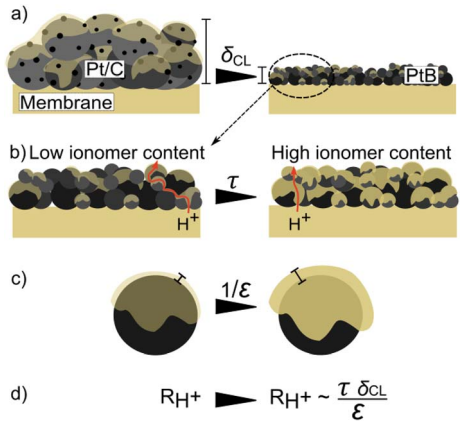

Fig. 3 Schematic of improvement steps to reduce protonic resistance R_{H^+} while ensuring proper gas transport through HC-based CLs: utilizing PtB instead of "standard" Pt/C (a) decreases CL thickness δ_{CL}, which (b and c) minimizes gas transport resistance even at higher ionomer volume fractions ε_i and additionally increases tortuosity τ. (d) Ultimately, a lower protonic resistance is achieved.

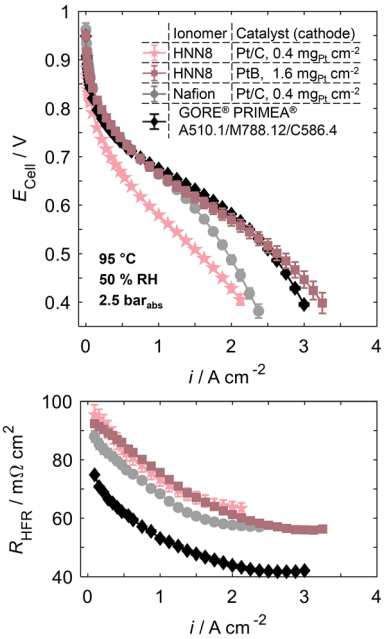

Fig. 4 Polarization curves and associated high-frequency resistance R_{HFR} of fully HC- and PFSA-based fuel cells with the following cathode compositions: star: Pemion® HNN8 with 50 wt% Pt/C (0.4 mg_{Pt} cm^{-2}, I/C = 0.2); square: Pemion® HNN8 with unsupported Pt (PtB, 1.6 mg_{Pt} cm^{-2}, 2.5 wt% dry ionomer in solids); circle: Nafion D2020 with 50 wt% Pt/C (0.4 mg_{Pt} cm^{-2}, I/C = 0.8); diamond: GORE® PRIMEA® MEA (0.1/0.4 mg_{Pt} cm^{-2} on anode/cathode; A510.1/M788.12/C586.4; thickness: 12 μm). All polarization curves were measured under 0.25/1 slpm (H_2/Air) at 50% RH, 95 °C, and 2.5 bar_{abs}.

disproportionately large improvements in protonic resistance while maintaining a proper gas transport resistance (Fig. 3).

At 50% RH, such a thin CL in HC-based fuel cells – utilizing HNN8 ionomer (similar to sPPB, but with a negligibly lower IEC; 2.5 wt% dry ionomer content) and PtB in the cathode (Pt loading: 1.6 mg_{Pt} cm^{-2}) – achieves a current density of 420 ± 22 mA cm^{-2} at 0.75 V (Fig. 4). This value is approximately 2.3 times higher compared to the best-performing HC-based MEA with Pt/C electrocatalyst, which achieves 180 ± 3 mA cm^{-2} at 0.75 V by using the same ionomer (*i.e.*, HNN8, cathode Pt loading: 0.4 mg_{Pt} cm^{-2}). At the same voltage, the current density of the PtB-based electrode is comparable to that of the self-made, fully PFSA-based reference (*i.e.*, 50 wt% Pt/C; Nafion D2020 ionomer, I/C = 0.8; cathode Pt loading: 0.4 mg_{Pt} cm^{-2}), which achieves 393 ± 18 mA cm^{-2} at 0.75 V. The peak power density (p_{max}) exceeds that of the self-made PFSA-based reference by 37% (see SI, Fig. S6a; p_{max}^{PFSA} = 0.98 W cm^{-2} *vs.* $p_{max}^{HC,\ PtB}$ = 1.34 W cm^{-2} *vs.* $p_{max}^{HC,\ Pt/C}$ = 0.86 W cm^{-2}). Overall, the PtB-based cathode achieves, for the first time under low-humidity conditions, performance comparable to that of a commercially available GORE® PRIMEA® MEA. This holds true despite the significant differences in HFR. Additional performance comparisons under higher gas inlet humidification are provided in the SI (Fig. S7b). Although the PtB loading is four times higher compared to the references used, the thickness of the PtB-based CL δ_{CL}, is significantly lower (Table 1). The high amount of unsupported Pt is necessary to compensate for the CL's fourfold lower ECSA. This, in turn, allows for reducing the kinetic overpotential, which is directly influenced by the roughness factor rf (Table 1).[33] However, a loading of 1.6 mg_{Pt} cm^{-2}, combined with the achieved power density, corresponds to a Pt specific power density of 1.2 g_{Pt} kW^{-1}. This remains well above the target set by the Japanese New Energy and Industrial Technology Development Organization[42] (NEDO, 0.19 g_{Pt} kW^{-1} by 2030) and the cost target defined by the U.S. Department of Energy[43] (DOE, maximum cost of a fuel cell system for heavy-duty transport of 80 $ kW^{-1}). These benchmarks highlight the need to reduce Pt loading while preserving the performance. When utilizing PtB in the cathode CL, future efforts may address the high Pt loading by increasing the ECSA of the unsupported platinum in the CL. Currently, only 40% of the CL's maximum attainable ECSA is utilized, where the maximum – 44 m^2 g^{-1} – is given by the BET-surface area of the PtB nanoparticles used. This limited utilization is likely due to PtB agglomeration within the CL, forming inactive or only partially active regions with insufficient ionomer contact for proton conduction and/or limited gas accessibility. As different commercially available PtB variants exhibit differing BET areas that result in varying ECSAs (see SI, Table S1), we anticipate that further improvements in catalyst utilization may result from optimizing ink dispersion. This can be effectively addressed by enhancing the sonication process (*e.g.*, SI, Fig. S9) and may be further improved by employing surfactants to reduce agglomeration and enhance Pt accessibility.

Compared to CLs utilizing Pt/C, as shown in Fig. 2, the thin HC-based PtB cathode exhibits the lowest protonic resistance while maintaining low oxygen transport resistance (Fig. 5). Additionally, compared to gas transport optimized hydrocarbon cathodes based on Pt/C (*i.e.*, cathodes utilizing 50 wt% Pt/C with an I/C ratio of 0.2), the PtB-based cathodes allow for approximately twice the ionomer volume fraction (Table 1) while exhibiting about three times lower tortuosity (see SI, Fig. S8). When applying defined upper threshold limits for oxygen

Table 1 Comparison of fully HC-based and fully PFSA-based fuel cells, utilizing Pemion® HNN8 and Nafion D2020 in the electrodes. The HC-based cathodes differ in terms of the electrocatalyst, with variations in carbon support, Pt loading, and thus in thickness δ_{CL} and roughness factor rf of the CL. Current density i was extracted from Fig. 2 (*i.e.*, at 50% RH and 0.75 V), while the ECSA was obtained from cyclic voltammetry measurements at ambient pressure, 40 °C, 96% RH and H_2/N_2 gas flows of 0.2/0 slpm. Mass activity i_m and specific activity i_s were measured under fully humidified conditions, H_2/O_2 gas flows (0.25/1 slpm), 1.5 bar_{abs}, and 80 °C

I/C ratio|dry ionomer volume fraction	Electrocatalyst	δ_{CL} (μm)	Pt loading (mg_{Pt} cm^{-2})	ECSA (m^2 g^{-1})	rf (cm^2 cm^{-2})	i_m (A g^{-1})	i_s (A m^{-2})	i (mA cm^{-2}) 0.75 V, 50% RH
0.8|14 vol% Nafion	50 wt% Pt/C	9.6 ± 0.7	0.40 ± 0.02	72 ± 2	288 ± 8	83 ± 5	1.2 ± 0.1	393 ± 18
0.2|6 vol% HNN8	50 wt% Pt/C	9.3 ± 0.5	0.40 ± 0.01	67 ± 3	268 ± 12	47 ± 3	0.7 ± 0.1	180 ± 3
—|14 vol% HNN8	100 wt% PtB	2.4 ± 0.8	1.60 ± 0.05	18 ± 1	288 ± 16	28 ± 4	1.6 ± 0.2	420 ± 8

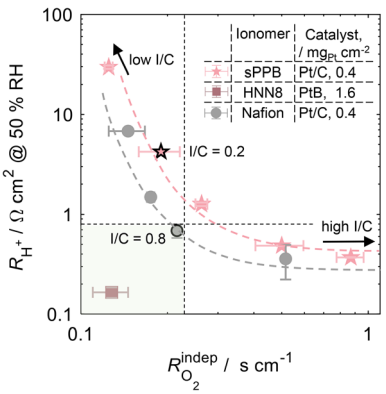

Fig. 5 Protonic resistance R_{H^+} (measured at 50% RH) *versus* pressure-independent O_2 transport resistance $R_{O_2}^{indep}$ (measured at 80% RH) for cathode CLs utilizing 50 wt% Pt/C (Pt loading of 0.4 mg_{Pt} cm^{-2}) and different contents of sPPB or Nafion D2020 (extracted from Fig. 2a and b, with black framed data points refer to the "standard" I/C ratio of operation). The square marked data point refers to a cathode CL utilizing 2.5 wt% Pemion® with unsupported Pt (PtB) loading of 1.6 mg_{Pt} cm^{-2}. All data points were measured at 80 °C.

transport resistance (Fig. 2b) and protonic resistance (Fig. 2d), an overlapping target window emerges in the plot of R_{H^+} *versus* $R_{O_2}^{indep}$, indicating the parameter space where both criteria are simultaneously satisfied. As seen in Fig. 5, only a few cathode compositions fall within this target area (green highlighted), with PtB being the only HC-based system.

Degradation of HC-based CLs: loss in rf

Repetitive load cycling events, with voltages constantly exceeding the onset potential of Pt oxide formation, lead to Pt dissolution and subsequent Pt redeposition.[44–49] As a consequence, the active Pt surface area is reduced. This reduction is most accurately traceable *in situ* as a loss in rf.[49] Referring to rf^{BOT} at the "beginning-of-test" (BOT), hydrocarbon-based cathodes utilizing PtB show a substantial loss of rf (~15%) over the first 100 cycles (Fig. 6a). This is in contrast to the carbon-supported reference (Pt/C), which only loses 4%, and may be related to a facilitated Pt reallocation due to the small distance between Pt particles, *i.e.*, a reduced ionic inter-particle resistance, and contributions of irreversible agglomeration.[50] Interestingly, the degradation in both HC-based cathodes utilizing HNN8 approaches with increasing cycles, particularly after cycles. This may stem from a countervailing effect, where the larger platinum particles in the PtB case exhibit a smaller surface-to-volume ratio that slows the degradation down. End-of-life, defined as a threshold of 60% rf by the US Department of Energy (DOE), is reached for HC-based cathodes utilizing Pt/C after approximately 7700 and for PtB already after about 4000 cycles (estimated by interpolation), highlighting the need for

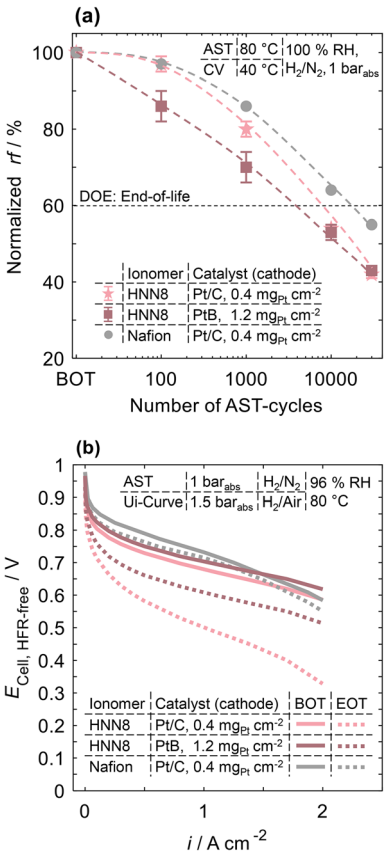

Fig. 6 (a) Normalized cathode roughness factor rf (rf/rf^{BOT}) as a function of AST-cycles, and (b) polarization curves at BOT and EOT of fully HC- and fully PFSA-based CCMs with varying cathode electrocatalyst. The cathodes utilize Nafion D2020 (I/C = 0.8, 50 wt% Pt/C, Pt loading of 0.41 ± 0.01 mg_{Pt} cm^{-2}) and Pemion® HNN8 with (i) 50 wt% Pt on high surface area carbon (Pt/C, 0.42 ± 0.02 mg_{Pt} cm^{-2}), and (ii) unsupported Pt (PtB, 1.2 ± 0.01 mg_{Pt} cm^{-2}).

further stabilization of PtB-based CLs. While these trends are important in emphasizing the potential of PtB in HC-based cathodes, a more pressing issue arises: under the current AST, even HC-based electrodes utilizing Pt/C exhibit a significantly greater loss in rf compared to Nafion-based references (I/C = 0.8, 50 wt% Pt/C). This loss is at least partially reflected in the recorded polarization curves (Fig. 6b), where the performance drop between BOT and EOT is significantly more pronounced for HC-based cells compared to Nafion-based references. The analysis suggests that the degradation behavior of HC-based cathodes may be fundamentally different from that of the Nafion systems and warrants a deeper mechanistic investigation.

Conclusion

In this study, platinum black was used as an unsupported electrocatalyst in hydrocarbon (HC)-based cathode catalyst layers to address the fatal tradeoff between gas transport resistance and protonic resistance at low humidity. Compared to carbon-supported electrocatalysts, PtB-based electrodes are not only unaffected by carbon corrosion of the support but allow for a reduction in both mass transport resistance and protonic resistance by severely reducing the thickness of the CL.

The performance improvements under dry conditions and elevated temperatures present a significant advancement for fuel cells with fully hydrocarbon-based CCMs (membrane and catalyst layer are both HC-based), exceeding the best-reported literature performance for PFSA-free PEM fuel cells[7] by 150% at application-relevant conditions (*i.e.*, 50% RH, 95 °C, 0.75 V). Despite the relatively high Pt loading of PtB-based cathodes, the ability to further increase the ECSA and overall performance underscores the potential of HC ionomers in fuel cells – particularly as their competitiveness against PFSAs under low-humidity conditions is demonstrated for the first time. While a reduction in PtB loading will be important to meet cost-related targets, especially in automotive applications where such benchmarks are already established, the findings also point to opportunities in sectors like aviation. In these contexts, the pressure to minimize platinum content is comparatively lower, making HC-based systems a promising route to avoid the use of environmentally concerning PFSAs. However, further advances in terms of platinum surface accessibility and lifetime stability remain essential to establishing the presented approach in multiple cells and stacks.

Author contributions

The contributions to this manuscript are listed in accordance with the CRediT taxonomy: H. Liepold (H. L.): writing – original draft, writing – review & editing, visualization, methodology, investigation, conceptualization. H. Sannemüller (H. S.): writing – review & editing, investigation. P. A. Heizmann (P. A. H.): writing – review & editing, writing – original draft, visualization, investigation. J. Stiegeler (J. S.): methodology. T. de Wild (T. W.): writing – review & editing, supervision. C. Klose (C. K.): writing – review & editing, supervision, resources. R. Alink (R. A.): writing – review & editing. S. Vierrath (S. V.): writing – review & editing, supervision, resources. S. Holdcroft (S. H.): writing – review & editing, resources. A. Münchinger (A. V): writing – review & editing, visualization, supervision, conceptualization.

Conflicts of interest

Steven Holdcroft is a co-founder and scientific advisor for Ionomr Innovations Inc., supplier of the Pemion® membranes and ionomer used in this work.

Data availability

Data supporting this article have been included as part of the SI. See DOI: https://doi.org/10.1039/d5se00809c.

Acknowledgements

The authors acknowledge funding from BMDV within the project 'H2Sky' (grant no. 03B10706G and 03B10706F).

References

1 M. Adamski, T. J. G. Skalski, B. Britton, T. J. Peckham, L. Metzler and S. Holdcroft, *Angew. Chem., Int. Ed. Engl.*, 2017, **56**(31), 9058–9061.
2 T. J. G. Skalski, B. Britton, T. J. Peckham and S. Holdcroft, *J. Am. Chem. Soc.*, 2015, **137**(38), 12223–12226.
3 D. A. Cullen, K. C. Neyerlin, R. K. Ahluwalia, R. Mukundan, K. L. More, R. L. Borup, A. Z. Weber, D. J. Myers and A. Kusoglu, *Nat. Energy*, 2021, **6**(5), 462–474.
4 C. Sonne, B. M. Jenssen, J. Rinklebe, S. S. Lam, M. Hansen, R. Bossi, K. Gustavson and R. Dietz, *Sci. Total Environ.*, 2023, **876**, 162770.
5 X. Lim, *Nature*, 2023, **620**(7972), 24–27.
6 M. Adamski, N. Peressin and S. Holdcroft, *Mater. Adv.*, 2021, **2**(15), 4966–5005.
7 H. Nguyen, D. Sultanova, P. A. Heizmann, S. Vierrath and M. Breitwieser, *Mater. Adv.*, 2022, **3**(23), 8460–8468.
8 H. Liepold, A. Bird, P. A. Heizmann, H. Fadlullah, H. Nguyen, C. Klose, S. Holdcroft, A. Kusoglu, S. Vierrath and A. Münchinger, *J. Power Sources*, 2024, **624**, 235537.
9 H. Nguyen, F. Lombeck, C. Schwarz, P. A. Heizmann, M. Adamski, H.-F. Lee, B. Britton, S. Holdcroft, S. Vierrath and M. Breitwieser, *Sustainable Energy Fuels*, 2021, **5**(14), 3687–3699.
10 H. Nguyen, C. Klose, L. Metzler, S. Vierrath and M. Breitwieser, *Adv. Energy Mater.*, 2022, **12**(12), 2103559.
11 H. Nguyen, J. Stiegeler, H. Liepold, C. Schwarz, S. Vierrath and M. Breitwieser, *Energy Technol.*, 2023, **11**(8), 2300202.
12 E. Balogun, S. Cassegrain, P. Mardle, M. Adamski, T. Saatkamp and S. Holdcroft, *ACS Energy Lett.*, 2022, **7**(6), 2070–2078.
13 E. Balogun, P. Mardle, H. Nguyen, M. Breitwieser and S. Holdcroft, *Electrochim. Acta*, 2022, **401**, 139479.
14 J. Peron, Z. Shi and S. Holdcroft, *Energy Environ. Sci.*, 2011, **4**(5), 1575.

15 C. Klose, T. Saatkamp, A. Münchinger, L. Bohn, G. Titvinidze, M. Breitwieser, K.-D. Kreuer and S. Vierrath, *Adv. Energy Mater.*, 2020, **10**(14), 1903995.
16 D. Yazili, E. Marini, T. Saatkamp, A. Münchinger, T. de Wild, L. Gubler, G. Titvinidze, M. Schuster, C. Schare, L. Jörissen and K.-D. Kreuer, *J. Power Sources*, 2023, **563**, 232791.
17 H. Liepold, H. Nguyen, P. A. Heizmann, C. Klose, S. Vierrath and A. Münchinger, *J. Electrochem. Soc.*, 2024, **171**(5), 54509.
18 V. Ramani, S. Swier, M. T. Shaw, R. A. Weiss, H. R. Kunz and J. M. Fenton, *J. Electrochem. Soc.*, 2008, **155**(6), B532.
19 M. Hwang, K. Nixon, R. Sun, C. Willis and Y. A. Elabd, *J. Membr. Sci.*, 2021, **633**, 119330.
20 J. E. Chae, S. J. Yoo, J. Y. Kim, J. H. Jang, S. Y. Lee, K. H. Song and H.-J. Kim, *Int. J. Hydrogen Energy*, 2020, **45**(57), 32856–32864.
21 S. Xu, M. Adamski, M. Killer, E. M. Schibli, B. J. Frisken and S. Holdcroft, *Macromolecules*, 2019, **52**(6), 2548–2559.
22 E. Balogun, M. Adamski and S. Holdcroft, *J. Electrochem. Soc.*, 2020, **167**(8), 84502.
23 M. Adamski, T. J. Skalski, E. M. Schibli, M. Killer, Y. Wu, N. Peressin, B. J. Frisken and S. Holdcroft, *J. Membr. Sci.*, 2020, **595**, 117539.
24 M. K. Debe, R. T. Atanasoski and A. J. Steinbach, *ECS Trans.*, 2011, **41**(1), 937–954.
25 M. Fikry, J. Herranz, S. Leisibach, P. Khavlyuk, A. Eychmüller and T. J. Schmidt, *J. Electrochem. Soc.*, 2023, **170**(11), 114524.
26 S. Gottesfeld and T. A. Zawodzinski. in *Advances in Electrochemical Science and Engineering*, ed. R. C. Alkire, H. Gerischer, D. M. Kolb and C. W. Tobias, Wiley, 1997, p. 195.
27 P. Costamagna and S. Srinivasan, *J. Power Sources*, 2001, **102**(1–2), 242–252.
28 E. A. Ticianelli, C. R. Derouin, A. Redondo and S. Srinivasan, *J. Electrochem. Soc.*, 1988, **135**(9), 2209–2214.
29 Ian D. Raistrick. in *Proceedings of the Symposium on Diaphragms, Separators, and Ion-Exchange Membranes*, ed. J. W. Van Zee, R. E. White, K. Kinoshita and H. S. Burney, The Electrochemical Society, Pennington, 1986, p. 172.
30 M. K. Debe, *ECS Trans.*, 2012, **45**(2), 47–68.
31 I. V. Zenyuk, P. K. Das and A. Z. Weber, *J. Electrochem. Soc.*, 2016, **163**(7), F691–F703.
32 D. R. Baker, D. A. Caulk, K. C. Neyerlin and M. W. Murphy, *J. Electrochem. Soc.*, 2009, **156**(9), B991.
33 K. C. Neyerlin, W. Gu, J. Jorne and H. A. Gasteiger, *J. Electrochem. Soc.*, 2006, **153**(10), A1955.
34 K. H. Kim, H. J. Kim, K. Y. Lee, J. H. Jang, S. Y. Lee, E. Cho, I. H. Oh and T. H. Lim, *Int. J. Hydrogen Energy*, 2008, **33**(11), 2783–2789.
35 D. Yazili-Marini, L. T. Fogang, E. Marini, T. Morawietz, G. Titvinidze, J. Bansmann, M. Hölzle and L. Jörissen, *J. Power Sources*, 2025, **641**, 236896.
36 J.-H. Choi, T. Agarwal, H. Park, J. Jung, A. Uddin, S. M. Ahn, J. M. Klein, A. S. Lee, M. Lehmann, C. Fujimoto, E. J. Park, T. Saito, R. L. Borup and Y. S. Kim, *ACS Energy Lett.*, 2025, 2392–2399.
37 K. A. Weber, C. S. Harzer, E. Bindl, K. Stengl and H. Gasteiger, *ECS Adv.*, 2025.
38 C. Schare, G. Titvinidze, N. Platenburg, M. Viviani, E. Cruz Ortiz, S. Vierrath, K.-D. Kreuer, C. Klose and A. Münchinger, *J. Mater. Chem. A*, 2025, **13**(25), 19292–19296.
39 K. C. Neyerlin, W. Gu, J. Jorne, A. Clark and H. A. Gasteiger, *J. Electrochem. Soc.*, 2007, **154**(2), B279.
40 N. Nonoyama, S. Okazaki, A. Z. Weber, Y. Ikogi and T. Yoshida, *J. Electrochem. Soc.*, 2011, **158**(4), B416.
41 P. Schneider, M. Batool, A. O. Godoy, R. Singh, D. Gerteisen, J. Jankovic and N. Zamel, *J. Electrochem. Soc.*, 2023, **170**(2), 24506.
42 New Energy and Industrial Technology Development Organization (NEDO), *Fuel Cell and Hydrogen Technology Development Roadmap: Fuel Cell Roadmap for FCVs/HDVs*, URL: **https://www.nedo.go.jp/content/800016621.pdf** 05.08.2025.
43 U. S. Department of Energy, *Multi-Year Program Plan*, **https://www.energy.gov/sites/default/files/2024-05/hfto-mypp-2024.pdf** 2024.
44 P. J. Ferreira, G. J. La O', Y. Shao-Horn, D. Morgan, R. Makharia, S. Kocha and H. A. Gasteiger, *J. Electrochem. Soc.*, 2005, **152**(11), A2256.
45 C. H. Paik, G. S. Saloka and G. W. Graham, *Electrochem. Solid-State Lett.*, 2007, **10**(2), B39.
46 E. Guilminot, A. Corcella, M. Chatenet, F. Maillard, F. Charlot, G. Berthomé, C. Iojoiu, J.-Y. Sanchez, E. Rossinot and E. Claude, *J. Electrochem. Soc.*, 2007, **154**(11), B1106.
47 L. Dubau, L. Castanheira, F. Maillard, M. Chatenet, O. Lottin, G. Maranzana, J. Dillet, A. Lamibrac, J.-C. Perrin, E. Moukheiber, A. ElKaddouri, G. de Moor, C. Bas, L. Flandin and N. Caqué, *Wiley Interdiscip. Rev.: Energy Environ.*, 2014, **3**(6), 540–560.
48 R. Borup, J. Meyers, B. Pivovar, Y. S. Kim, R. Mukundan, N. Garland, D. Myers, M. Wilson, F. Garzon, D. Wood, P. Zelenay, K. More, K. Stroh, T. Zawodzinski, J. Boncella, J. E. McGrath, M. Inaba, K. Miyatake, M. Hori, K. Ota, Z. Ogumi, S. Miyata, A. Nishikata, Z. Siroma, Y. Uchimoto, K. Yasuda, K.-I. Kimijima and N. Iwashita, *Chem. Rev.*, 2007, **107**(10), 3904–3951.
49 R. K. F. Della Bella, B. M. Stühmeier and H. A. Gasteiger, *J. Electrochem. Soc.*, 2022, **169**(4), 44528.
50 L. Fan, J. Zhao, X. Luo and Z. Tu, *Int. J. Hydrogen Energy*, 2022, **47**(8), 5418–5428.